The effect of creep in the ‘4 de Abril’ cable-stayed bridge

Diogo Drumond Dias

Department of Civil Engineering, Architecture and Geo-Resources Superior Técnico, Universidade de Lisboa, Avenida Rovisco Pais, 1, 1049-001 Lisboa, Portugal

ABSTRACT

Concrete exhibits a viscoelastic-plastic material behaviour, i.e., when submitted to stress, it shows an instantaneous elastic response and then a viscoplastic deformation through time. The first studies about shrinkage were made in 1900, by Considère, and the creep concept was presented in 1905, by Woolson. Since then, several theories and models were developed, leading to today’s accurate modelling of concrete long-term behaviour.

The long-term behaviour of concrete has a large application field being particularly relevant in the analysis and design of prestressed concrete bridges. An incorrect evaluation of the latter can potentiate excessive deformation in the spans, cracking and prestress losses. Different studies reveal that predictions of long-term behaviour in concrete structures can significantly differ from the real response. The non-homogeneity of concrete properties, increased by the variability of environmental conditions, like moisture and temperature, combined with the internal forces variation during construction are the main factors contributing to that discrepancy.

This main goal of this thesis was the evaluation of the accuracy of three creep prevision models, adopted in the main concrete structures codes when applied to cable-stayed concrete bridges. In this context, the “4 de Abril” bridge was selected as case-study, and an analysis including the constructive phase and the subsequent 20 years was conducted. A three-dimensional numerical model was created using ABAQUS software, which was calibrated and validated with on-site values provided from the structure’s monitoring system.

It was concluded that creep prediction models overestimate the material’s behaviour and are less reliable for multiaxial loaded elements.

Keywords: Concrete, cable-stayed bridges, creep, shrinkage, numerical modelling, codes.

1. Introduction

At early ages, the deformation of a concrete element experiences is mostly due to drying shrinkage. If submitted to load, it will also experience an increase of deformation through time, called creep. Despite the convenience of dissociating long term deformation into shrinkage and creep, these phenomena are predicted by models based in theories that assume these two phenomena to be interdependent.

The mechanism of shrinkage was firstly divided into two phases by Hobbs (1974). CEB (1993) divides this mechanism into a deformation occurring before concrete hardening and a deformation taking place afterwards. The first is known as ‘plastic shrinkage’ and is due to water evaporation at the concrete elements’ surface. The main percentage of shrinkage occurs after concrete hardening and, despite of being usually associated to drying shrinkage, it is also a consequence of other factors like autogenous, chemical, thermic and carbonation shrinkage. Drying shrinkage in concrete elements occurs mainly due to the exposition to non-saturated environments with constant temperature and relative humidity (Bazant, 1988). Concrete’s drying brings a continuous loss of the adsorbed and zeolitic water in the cement paste. It results in a capillary stress reduction, balanced by an increase of compressions in the microstructure, resulting in a volume reduction through time (Dias-da-Costa, 2006).

The mechanism of creep is originated in the hardened cement paste submitted to considerable stresses and also in breaking the bonds between the aggregates and the cement paste (Bazant, 1988).

Creep, from a microscopic perspective, can be described as the division into basic and non-basic components. The first one is an intrinsic material property that can only be determined experimentally with a uniform distribution of the humidity inside the element (Dias-da-Costa, 2006). The non-basic creep also called “drying creep” or “Pickett effect” occurs in drying concrete elements. This continuous process

leads to an increment on the number of cement gel bonds, increasing the hardened cement paste volume.

To the non-basic creep component contributes the high capillarity of the cement paste, associated to the strongly hydrophilic layers of hydrated calcium silicates, bonded by very unstable and disordered layers of cement paste. It is expected that creep deformation may lead to changes in the solid structure, with displacements enabling solid particles diffusion, from highly stressed regions onto more stable microstructure areas. The disjunction pressure, due to the presence of adsorbed water, weakens the bonds, contributing to the reduction of creep after cement paste drying (Bazant and Wittman, 1982).

Bazant *et al.* (1997) presented the microprestress-solidification theory for concrete creep, currently adopted to model the effects of long-term aging and drying of concrete. For concrete at earlier ages, this theory justifies the time-dependent variation of viscosity with the gradual deposition of new layers of hydration products in micropores walls.

The cement paste hydration is a short-living process, and Bazant *et al*. (1997) justify the long term aging with viscous shear slips between opposite micropores walls, where bonds and bridges that cross the micropores break and reform with adjacent atoms. This process leads to a relaxation of the tensile microprestress, normal to the slip plane and transferred through bonds and bridges, resulting in a creep rate decrease. The microprestress is originated by the disjoining pressure in the micropores, due to the hindered adsorbed water and also by highly localized volume changes, caused by hydration or drying.

According to the microprestress solidification theory, changes in the relative humidity of capillary pores are also responsible for changes in the micropores disjoining pressure, resulting in Pickett effect (drying creep) (Bazant *et al*., 1997).

The study of concrete long-term behaviour has a large application in elements subjected to bending, like prestressed concrete bridges, since it may lead to an excess of deformation / curvature in the mid-spans, cracking and prestress losses. Several studies reveal that, in concrete structures, long-term behaviour prediction analysis can significantly differ from the real response Rito (2016). The variation of internal forces, during the construction phase, and the non-homogeneity of concrete properties, increased by the variation of environmental conditions, such as moisture and temperature changes, are the main factors to that discrepancy.

This paper describes a numerical study conducted to evaluate the accuracy of the creep prediction models adopted by Eurocode 2 (CEN, 2005), Model Code 90 (CEB-FIP Model Code, 1993) and Model Code 2010 (fib Model Code, 2010) codes. These codes were applied into a case-study: the '4 de Abril' bridge, a concrete cable-stayed bridge in Angola.

The study described in this paper was performed with the aim to evaluate the accuracy of the creep prediction models adopted by Eurocode 2 (CEN, 2005), Model Code 90 (CEB-FIP Model Code, 1993) and Model Code 2010 (fib Model Code, 2010).

2. Description of the "4 de Abril" bridge

The "4 de Abril" bridge over the Catumbela river, in Angola, links Benguela to Lobito. The construction started in May 2007 and ended in July 2009.

This concrete bridge, Fig. 1, has three cable-stayed spans, a central one with 160.0 m and two side spans with 64.0 m each, and access viaducts at both river sides with 90.0 m and 60.0 m length each, divided in 30.0 m span. This construction has a total length of 438.0 m.

Fig. 1 – View of the "4 de Abril" bridge.

The cables are spaced 8,00 m, disposed in semi-harp and attached to two "U"-shaped pylons 46.0 m height and longitudinally anchored in two solid zones, designed to dissipate the huge forces applied by the cables' anchorages (Rito *et al*., 2009).

The deck is in C35/45 concrete and it comprises mainly two large longitudinal beams, lightened with cylindrical hollow moulds. The beams are connected between themselves by a slab and, along its deployment, with prestressed transversal beams 4.0 m apart.

The "U"-shaped pylons were built in reinforced and prestressed C35/45 concrete and their masts are

hollow. Each pylon foundation includes 16 piles with a diameter of 1.2 m and pile caps connected to a prestressed cross-beam, providing stiffness to the assemblage.

The bridge's deck was cantilevered constructed in sequence leads, using two pairs of falsework and formwork to cast each segment of the deck (4.0 m each). The viaducts were cast span-by-span on traditional falsework.

This bridge is equipped with a sophisticated monitoring system allowing recording both material and structural behaviour.

The time-dependent behaviour of the bridge's concrete was analysed measuring the long-term deformation of several specimens stored at the structure, some of these submitted to constant axial load, this way enabling the division of the total strain into elastic, creep and shrinkage deformation.

The bridge's structural behaviour is monitored in two transversal sections of the deck using 9 vibrating wire strain gages placed inside the suspended middle span section, S1, and by another 9 placed at the transversal section located 14.5 m from the North tower, S2. At both sections, 5 strain gages are placed near the top surface and the other 4 near the bottom surface, according to Fig. 2.

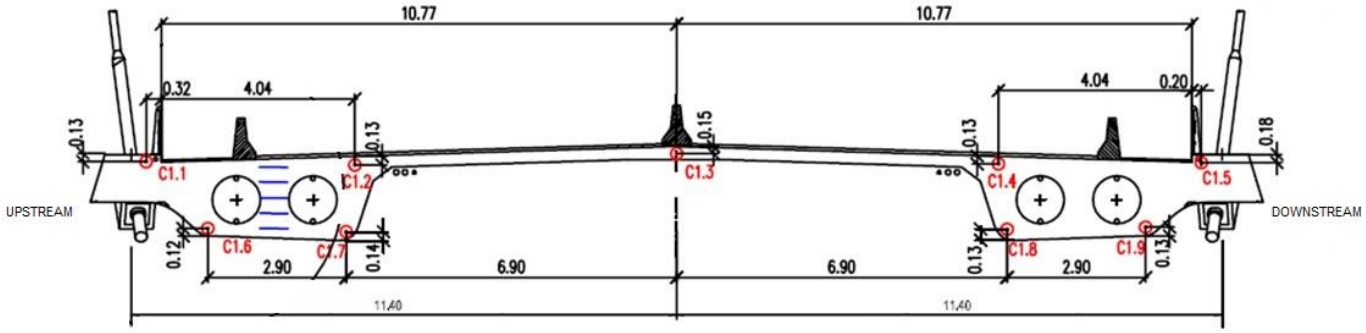

Fig. 2 – Disposition of the vibrating wire strain gages at cross-section S1 (LNEC, 2009).

3. Description of the numerical model

a. Objective and methodology

The objective was to simulate the long-term behaviour of concrete cable-stayed bridges, applied to the '4 de Abril' bridge. The methodology followed to reach the latter has been the following:

(1) To analyse the long-term data recorded from on-site concrete specimens;

(2) To build a numerical model to reproduce the material behaviour with a custom viscoplastic deformation using user-defined prediction laws;

(3) To build a three-dimensional model of the "4 de Abril" bridge;

(4) To calibrate the numerical model using the data from the on-site static loading tests;

(5) To simulate the bridge's long-term behaviour using user-defined prediction laws adopted in codes and another one based on the average material behaviour.

b. Finite element models

The numerical models were built using the finite element program ABAQUS 6.14. The geometry of the structure was defined based on plans and sectional drawings (Fig. 2 and Fig. 3) allowing the generation of two-dimensional (Fig. 4) and three-dimensional (Fig. 5) finite element models.

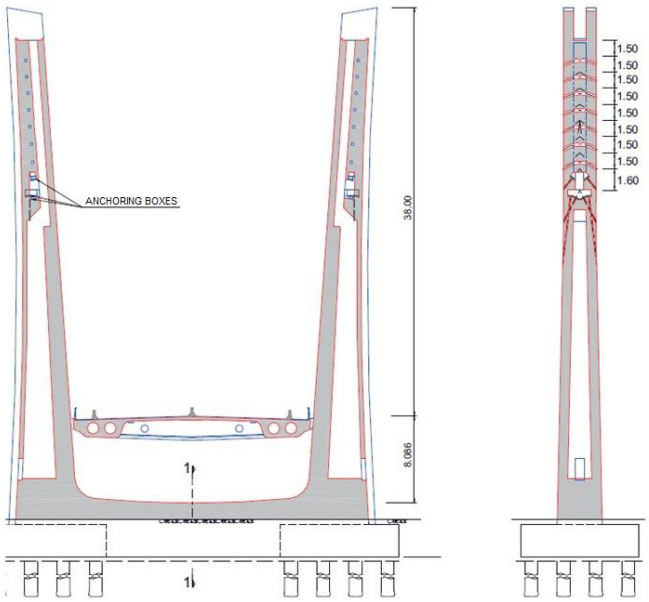

Fig. 3 – Transversal and longitudinal plans of the bridge's tower (Braga and Lopes, 2009).

Besides the cable-stays, modelled using three-dimensional deformable wire elements, all the other

Fig. 4 – Two-dimensional numerical model.

components were modelled using three-dimensional solid deformed elements.

The boundary conditions consisted in two different support conditions. The structure's main support is positioned on the base of the pile caps. It was considered a built-in support, to reproduce the effect of the 16 piles under each mast. The remaining boundary conditions define the bridge's abutments and the columns supporting the access viaducts, in both sides of the river, in which the vertical and transversal displacements were restrained.

The remaining boundary conditions define the bridge's abutments and the columns supporting the access viaducts, in both sides of the river. The vertical and transversal displacements, as well as the rotations in all directions were restrained.

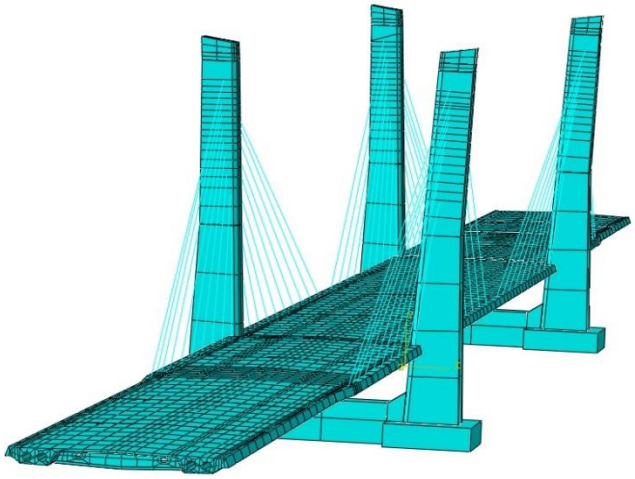

Fig. 5 – Mesh applied to the three-dimensional numerical model.

Except the connections between cables and masts and between cables and deck, that were modelled using a coupling constraint, restraining only the displacements, all the other connections were defined using a tie constraint with a surface-to-surface interaction, restraining the differential deformation between the connected elements.

The bridge erection phase was modelled associating the analysis steps to the "model change" option, knowing the information about the construction schedule and the cable tensioning values. This last information was modelled with a predefined field based on an equivalent temperature variation.

The structural loading was defined with the dead-weight and with other permanent loads located on the upper surface of the bridge's deck.

The three-dimensional mesh was built using 4-node tetrahedral elements with dissimilar size meshes for different structural elements in order to minimize computation time, given an acceptable numerical error.

The structural behaviour is also influenced by the material properties. The cable-stays were defined with a Young's modulus (E) of 190 GPa and a Poisson ratio (ϑ) of 0.30 and a resultant shear modulus (G) of 79.2 GPa. Despite the complexity associated to all ordinary and prestress reinforcement in the bridge's deck, all the components used to define the deck's structural elements were assumed homogeneous, with current Poisson ratio, equivalent Young's modulus and equivalent shear modulus. The latter two were calibrated based on a parametric study.

c. Models calibration and validation

As previously mentioned, the models' calibration consisted in setting up an equivalent Young's modulus and an equivalent shear modulus capable of reproducing the measured structural response. This calibration was performed with the monitoring data on the vertical displacement from the on-site static loading tests, using hydrostatic levelling systems that were placed at I, K, O and Q as shown in points in Fig. 6.

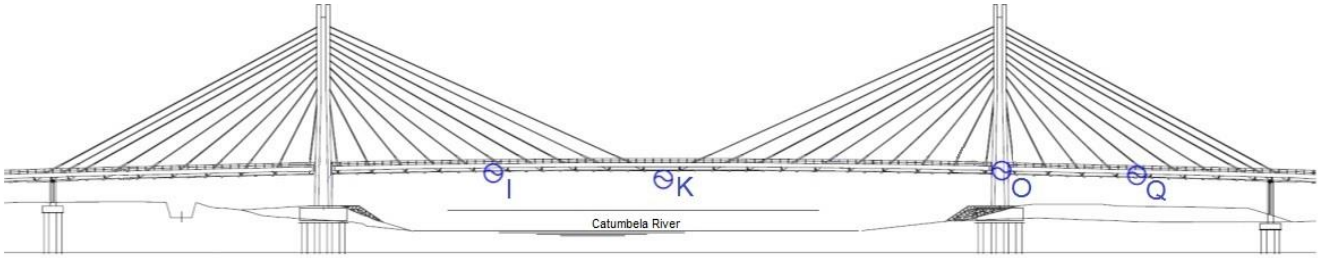

Fig. 6 – Longitudinal placement of the hydrostatic leveling systems.

These tests were executed after the construction phase and were composed by a transversal line of four loaded trucks (reproduced in Fig. 7-a), totalling 1277 kN.

The study was firstly performed with a static analysis in a simpler two-dimensional model of the "4 de Abril" bridge. Then, the resulting equivalent material values were applied to the three-dimensional model. The loading tests were also modelled in the 3-D model (Fig. 7-b), validated with the comparison between the obtained bridge's deck vertical displacement and the values from the 2-D model and from the monitored structural behaviour.

Fig. 7 – Static loading tests: on-site (a) and in the numerical model (b).

From the parametric study performed with the 2-D model, an equivalent Young's modulus of 39.8 GPa and an equivalent shear modulus of 16.6 GPa ($\vartheta = 0.2$) were settled.

With the 3-D model, the influence of a possible eccentricity, assumed as 0.3 m, of the truck's wheels during the static loading was analysed. Table 1 shows the error between the real vertical displacement, measured with the hydrostatic levelling systems, and the values obtained with the same loading cases in the 2-D and 3-D models (centered and eccentric loading). The results show a good agreement between the real measured values and the centered loading case in the 3-D model (mean error of 8.3%).

Table 1 – Error between the numerical and measured displacement values.

	Two-dimensional model		Tri-dimensional model			
			Centered loading		Eccentric loading	
	Error	Average error	Error	Average error	Error	Average error
I	6,2%	15,7%	3,6%	8,3%	16,9%	36,3%
K	2,9%		7,2%		18,5%	
O	47,8%		21,1%		94,4%	
Q	5,8%		1,2%		15,3%	

The bridge's deck long-term behaviour was defined by creep prediction laws, written in Fortran language and then implemented in the bridge's finite element model. Those laws were firstly calibrated to best reproduce the concrete long-term creep deformation, monitored on-site.

The comparison between the experimental and the theoretical creep coefficient values ($\varphi(t, t_0)$) is displayed in Fig. 8. It is concluded that these last values overestimate concrete creep. This discrepancy might be explained through the differences in the local relative humidity and temperature over time, once it was considered uniform and equal to the average of the monitored values in the codes formulation. The difference between the creep coefficient evolution in the three monitored specimens reproduce the material response variability.

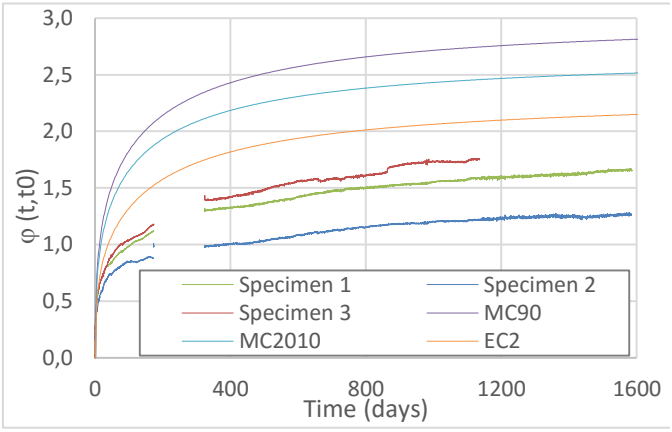

Fig. 8 – Comparative analysis between the creep coefficient from the experimental data and from the creep laws applied to a numerical specimen.

The creep law adopted in Eurocode 2 (CEN, 2005) represents the best approach to the material behaviour. It was also defined a new creep prediction law, obtained by adjusting some coefficients from the Eurocode 2 formulation, in order to best represent the average concrete creep behaviour, aiming at improving the prediction of the long-term structural behaviour.

4. Results

a. Long-term structural behaviour

The 20 year structural analysis performed to the three-dimensional model of the "4 de Abril" bridge was carried out to assess if the creep prediction laws adopted by EC2, MC90 and MC2010 are able to reproduce with good approximation the strains monitored with the 9 strain gages positioned in S1 and S2 sections.

The strain gages, represented in Fig. 2, measured the total strains evolution in the deck's longitudinal direction (ε_{33}). Fig. 9 and Fig. 10 present the comparison between measured values and those extracted from the numerical analysis in sections S1

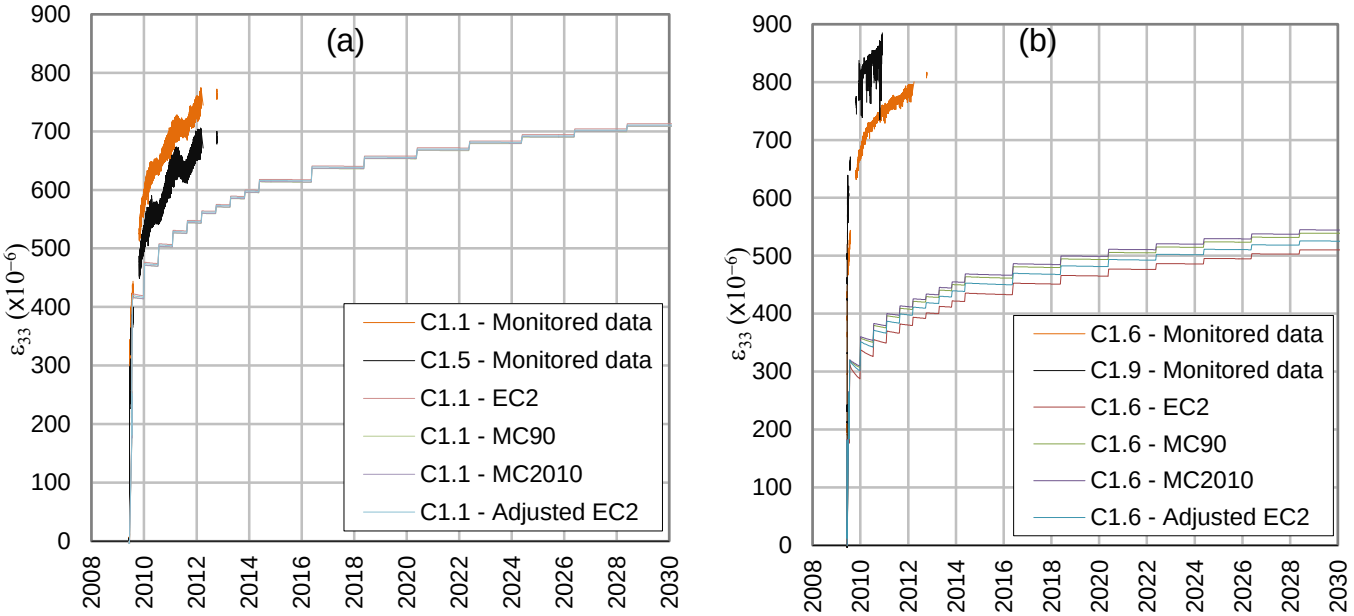

Fig. 9 – Comparison between the experimental data and the total strains in the longitudinal direction (ε_{33}) from the numerical analysis in an upper (a) and lower (b) fibre of section S1.

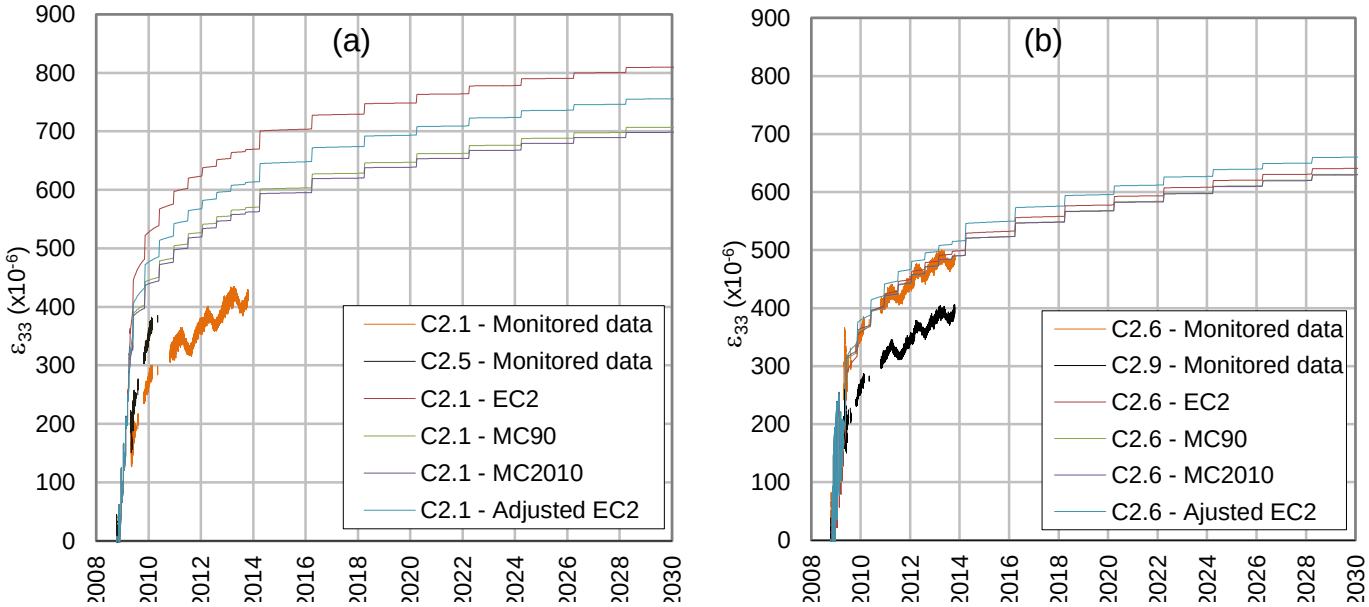

Fig. 10 – Comparison between the experimental data and the total strains in the longitudinal direction (ε_{33}) from the numerical analysis in an upper (a) and lower (b) fibre of section S2.

and S2, respectively. Each figure illustrates the measurements in an upper (C1.1/C2.1) and lower fibre (C1.6/C2.6), illustrated in Fig. 11.

In section S1 (Fig. 9), subjected to a positive bending moment, the results from the numerical analysis are clearly underestimated, compared to the monitored data. This difference is upper (Fig. 9-a) in the lower fibre (Fig. 9-b), subjected to positive stresses that may lead to concrete cracking, further increasing the longitudinal strains. This deformation increase has not been taken into account in the concrete material modelling.

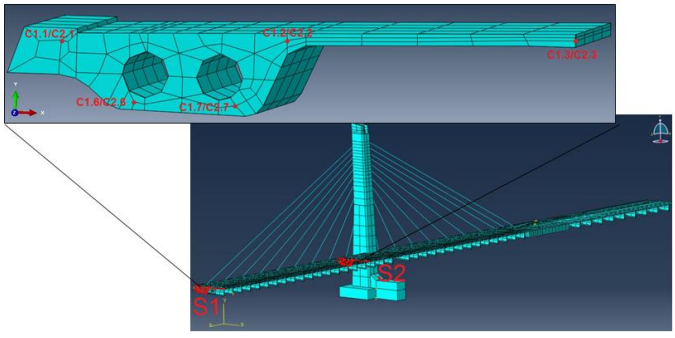

Fig. 11 – Selected fibres in each section.

The discrepancy shown in section S1 fibres (Fig. 9) may also be due to the fact of not having considered long-term prestress losses in the cables, which would also lead to deformation increase in the bridge's deck middle span.

Despite the discrepancies presented in both sections, the numerical analysis results are very similar for the three codes prediction laws and also for the law adjusted from EC2 approach. The EC2 give the best prediction for the upper fibre (C1.1), and MC2010 for the lower fibre (C1.6). The adjustments made to the EC2 code have not contributed to significant improvements.

The strains values in section S1 (Fig. 9) are significantly higher than the values obtained for section S2 (Fig. 10). This difference may be due to the fact that, after the conclusion of the construction phase, concrete's long-term behaviour effects transfer part of the internal forces, resulting from bending moment, to the central middle span, designed only with continuity prestress.

The results from the numerical analysis show reasonably good approximations to the monitored data for the section S2 (Fig. 10). The comparison between numerical and experimental data shows some inconsistency. Prediction laws overestimate the upper fibre (C2.1 in Fig. 10-a) strain values and underestimate the total strains in the lower fibre (C2.6 in Fig. 10-b). The inconsistency is also noticed when comparing C2.1 with other upper fibres (C2.2 and C2.3 in Fig. 2) once, unlike C2.1, it is observed lower estimates in the latter two fibres.

For all the upper fibres (e.g. C2.1) the EC2 and MC2010 creep prediction laws provide the higher and lower values of strains, respectively. For the lower fibres (e.g. C2.6) the highest and best prediction values result from the analysis performed with the concrete viscoplasticity law adjusted from EC2.

b. Long term structural effects

The structural analysis are supported and complemented with the structural effects evolution, especially the vertical displacement in the suspended middle span and the evolution of the creep coefficient ($\varphi(t, t_0)$).

The vertical displacement evolution through time leads to a deflection increase at the deck's suspended middle span. Despite this consequence of the concrete's concrete long-term behaviour effects is not part of the bridge's long-term monitoring program, it was analysed in the numerical model, as an attempt to foresee the progress during the bridge's first 20 years.

The Fig. 12 shows, according to the EC2 creep prediction law, the numerical model deformed shape at the end of the 20 year differed analysis. It is possible to see several inflexion points in the bridge's deck, and to identify the vertical displacement highest value to occur in the suspended middle span.

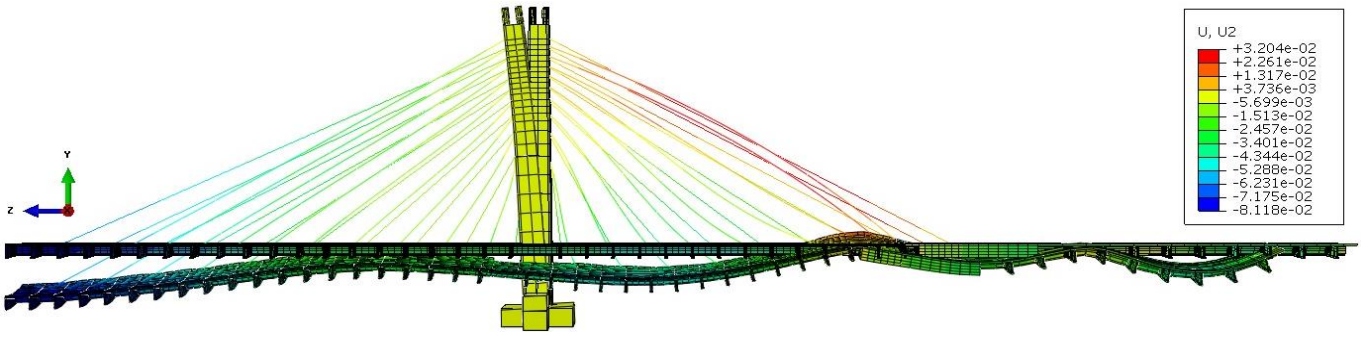

Fig. 12 – Deformed shape, (with a scale factor of +100) superimposed to the numerical model non-deformed shape, according to the EC2 code application.

The graph in Fig. 13 displays the evolution, until 2030 year, of section S1 vertical displacement, since concreting of the deck's closing segment. The values represent the average vertical displacement measured in the 5 fibres analysed in this section.

At the end of the construction phase (approximately June 2009), the vertical displacement in the middle span is approximately 60 mm (downwards). As shown in Fig. 13, in 2030 the largest vertical displacement results from the MC90 prediction, with an estimate 77 mm. The adjusted EC2 creep prediction law results in a lower value, a little over 70 mm. The other two creep code (MC2010 and EC2) present intermediate displacement values.

The creep coefficient ($\varphi(t, t_0)$) can easily be obtained dividing the numerical creep strains by the elastic strains. Fig. 14 and Fig. 15 show the creep coefficient, measuring the evolution of the creep

strain, in the longitudinal direction of sections S1 and S2, respectively.

It is important to refer that, as mentioned in section 4.a., this model does not consider the steel cables long-term prestress losses. This factor may lead to conservative values of the vertical displacement.

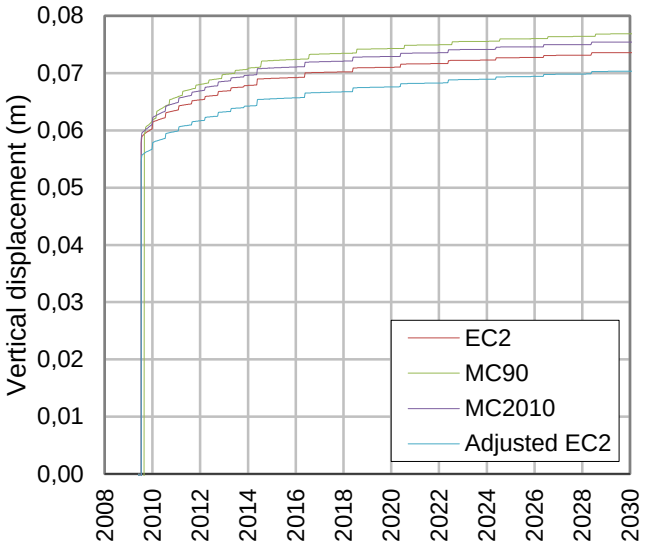

Fig. 13 – Average vertical displacement token from the numerical analyses in section S1.

The comparison between the creep coefficient evolution in the longitudinal direction ($\varphi_{33}(t,t_0)$) in both sections reveals lower values for the suspended middle span section (S1). This might be due to the higher compressive stresses, verified in the other cross-section (S2), caused by the cables tension horizontal components sum.

Fig. 14-b indicates that S1 lower fibres are subjected to unexpected low creep strains (lower than the elastic strains), corroborating the large discrepancy between the numerical results and monitored data in Fig. 9-b. The noticeable differences, between the creep prediction laws for this section, indicate that these were not calibrated for elements subjected to bending moments.

The structural analyses in section S1, located in the middle span, led to higher transversal stresses than longitudinal stresses in the bridge's deck. This fact might have some influence in the creep strain evolution, since Abaqus viscoplastic computation favours direction subjected to the higher stress values.

The longitudinal creep coefficient evolution ($\varphi_{33}(t,t_0)$), obtained through the long-term numerical analyses, of section S2 upper (Fig. 15-a) and lower fibres (Fig. 15-b) is quite closer to the values obtained from the concrete's long-term behaviour (Fig. 8).

According to Fig. 15, it is also possible to verify that, when creep prediction laws are applied to a cross-section only submitted to compressive stresses, differences between measured and predicted values become quite lower.

As shown in Fig. 14 and Fig. 15 the higher longitudinal creep coefficient values resulting from the application of EC2 and adjusted EC2 creep models. The remaining MC90 and MC2010 creep laws lead to lower coefficients, inappropriate for elements subjected to tension stresses (Fig. 14-b), happening only because the numerical model does not contemplate the deck's continuity prestress in the middle span.

Fig. 16 presents the longitudinal stress evolution of a section S1 lower fibre. The results indicate that, through time, the lower fibres will be submitted to a higher stress, approaching C35/45 tensile strength (f_{ctm}=3,2MPa). As a consequence, if the continuity prestress were not considered in the deck's closing segment, the deck's lower fibres will possibly crack due to the structure long-term behaviour.

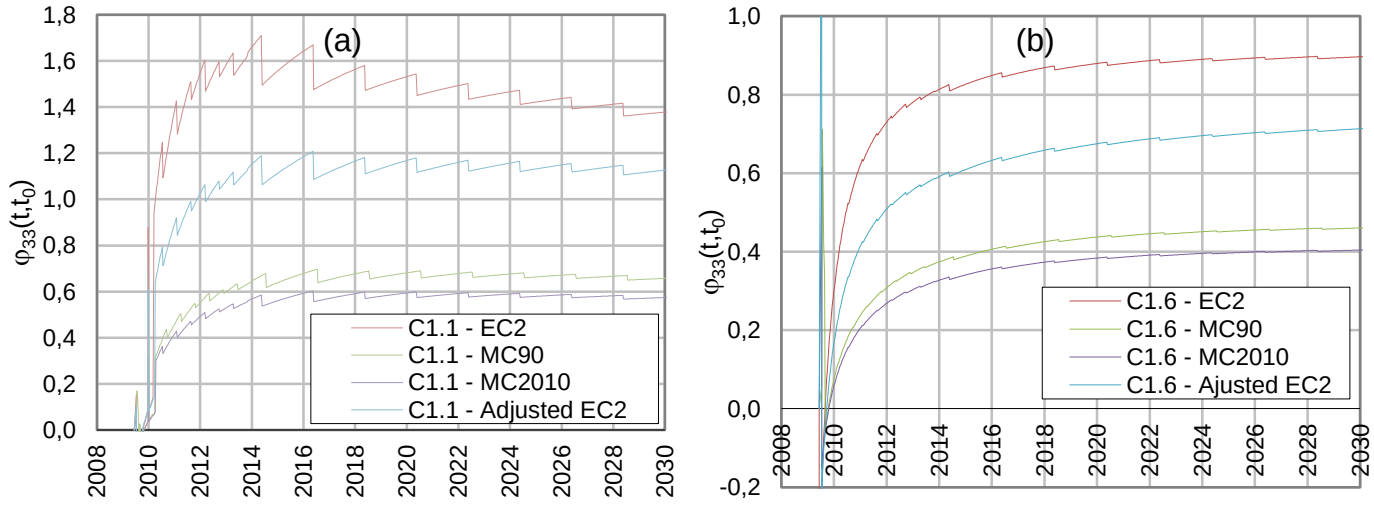

Fig. 14 – Creep coefficient evolution ($\varphi_{33}(t,t_0)$) according to the numerical analyses in a upper (a) and lower (b) of section S1.

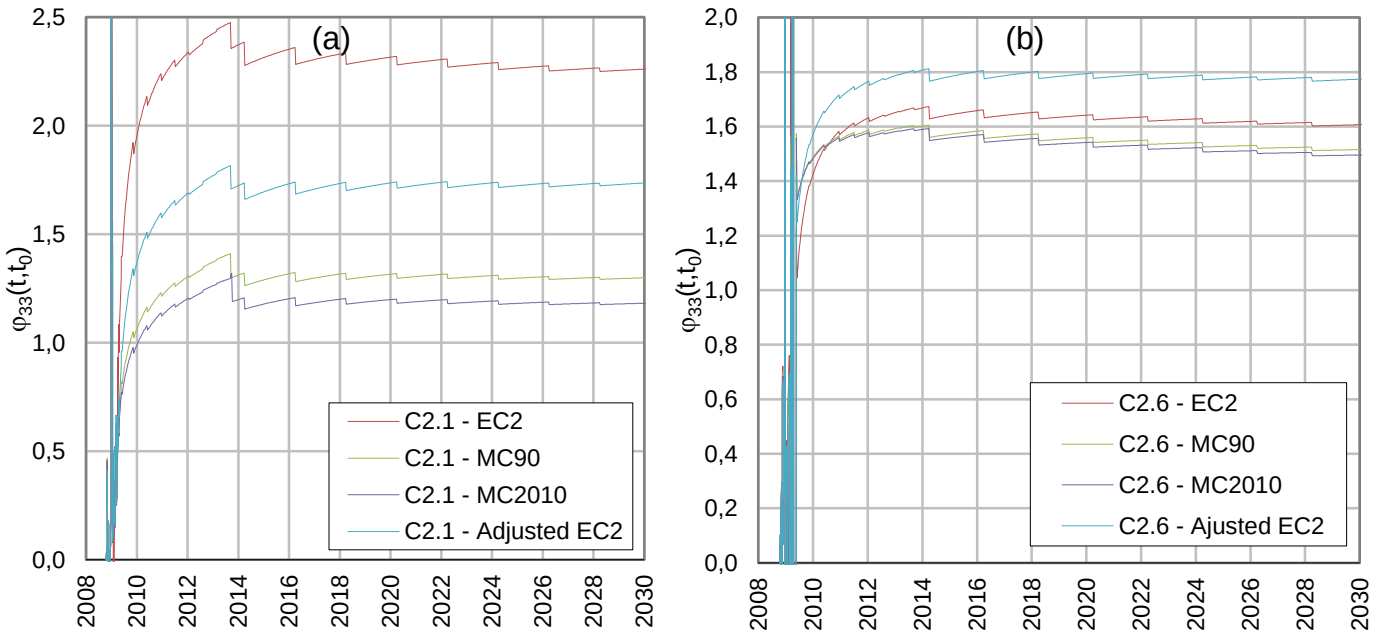

Fig. 15 – Creep coefficient evolution ($\varphi_{33}(t,t_0)$) in the longitudinal direction according to the numerical analyses in a section S2 upper (a) and lower fibre (b).

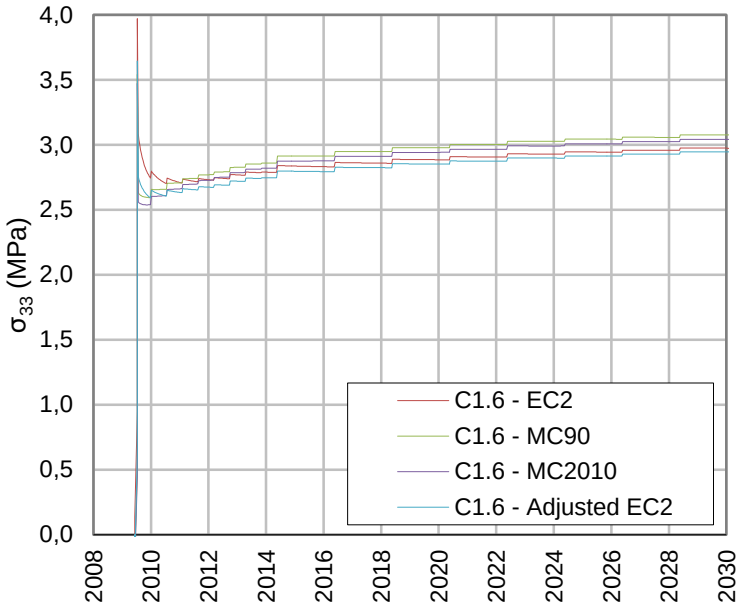

Fig. 16 – Longitudinal stress evolution ($\sigma_{33}(t)$) according to the numerical analyses in a section S1 lower fibre (b).

5. Discussion of results and conclusions

A 3-D and a 2-D numerical models of the '4 de Abril' bridge, capable of simulating its behaviour from the construction phase up to a large time horizon, were developed using the finite element software Abaqus, calibrated based on data from the static loading tests, conducted immediately after the construction.

It was concluded that the 3-D model is more accurate than the 2-D model. It was also concluded that, during the static loading analyses, the trucks did not deviate from the defined track.

The long-term analyses, based on MC90, MC2010, and EC2 creep prediction laws, were firstly calibrated and validated using creep tests data. All these prediction laws overestimate the average material behaviour recorded, with EC2 leading to the best analysis approach.

The long-term structural analyses were performed for the first 20 years after the construction start. The weaker numerical results take place in areas where the deck's transversal section is not entirely submitted to compressive stresses.

The comparison between the monitored data and the numerical results shows that the largest differences are observed at the fibres submitted to tension stresses. This might have some influence on the long-term behaviour, being expected higher values for the vertical displacement in the deck's middle span.

It was observed that the creep prediction laws only result in acceptable values for elements subjected to higher stresses in a preferential direction, like the specimen and section S2, both subjected to a high axial stress. Section S1 fibres, on the contrary, are submitted to a multiaxial stress state with similar values in the longitudinal (low value of positive longitudinal bending moment) and transversal directions (transversal internal forces distribution of the desk permanent loads).

The results for the transversal section in the suspended middle span – section S1 – show a considerable underestimation of the longitudinal total strains (ε_{33}), having discrepancies in the order of magnitude verified by Rito (2016) in a similar study. The differences between the numerical analyses and the monitored data may be due to the non-consideration of the long-term prestress losses in the stayed-cables.

The results from the numerical analyses show reasonably good approximations to the monitored data for section S2 (Fig. 10), that is entirely submitted to compressive stresses, resulting from the sum of the horizontal stayed-cables components.

It is possible to conclude that, despite not being able to reproduce the tensioned fibres behaviour, the best long-term analysis results from the EC2 creep prediction law.

This paper reveals that is crucial to improve the current creep prediction models, extending the application field. It is suggested improvements in the sensibility to triaxial loads and bending solicitations, once the main problem was the reproduction of the long-term behaviour in tensioned fibres.

References

Bazant, Z. P. (1988). *Material Models for Structural Creep Analysis*. Mathematical Modeling of Creep and Shrinkage of Concrete.

Bazant, Z. P., Baweja, S., Hauggaard, A. B., & Ulm, F.-J. (1997). *Microprestress-solidification Theory for Concrete Creep. I : Aging and Drying Effects*. Journal of Engineering Mechanics, 123, 1188–1194.

Bazant, Z. P., & Wittman, F. H. (1982). *Creep and Shrinkage in Concrete Structures*. Wiley-Interscience, (Creep and Shrinkage Concrete Structures Mathematical Models for Creep and Shrinkage of Concrete), 164–256.

Braga, Ó. L., & Lopes, F. (2009). *Ponte 4 de Abril, 4th of April Bridge*. Governo de Angola.

CEB. (1993). *Structural Effects of Time-dependent Behaviour of Concrete: Revision of the Design Aids of the CEB Design Manual* in Accordance with the CEB-FIP Model Code 1990. le Comité.

CEB-FIP Model Code. (1993). *Model Code 1990 - Design Code*. Lausanne, Switzerland: Thomas Telford House Ltd.

CEN. (2005). *Eurocode 2 - Design of concrete structures* - Concrete Bridges - Design and detailing rules. Brussels: CEN - European Commitee for Standardization.

Dias-da-Costa, D. (2006). Comportamento Diferido do Betão - *Modelação Numérica do Comportamento de Fluência de Vigas em Betão de Alta Resistência.* Tese de Mestrado em Engenharia Civil. Departamento de Engenharia Civil da Universidade de Coimbra.

fib Model Code. (2010). *Model Code 2010 - First complete draft* (1st ed.). Lausanne, Switzerland: International Federation for Structural Concrete (fib).

Hobbs, D. W. (1974). *Influence of Aggregate Restraint on the Shrinkage of Concrete*. *Journal Proceedings,* 71(9), 445–450.

LNEC, I. P. (2009). *Ensaios de Carga da Ponte 4 de Abril sobre o Rio Catumbela na Via Rápida entre Benguela e Lobito em Angola.*

Rito, A. (2016). Concepção e Construção. Armando Rito Engenharia SA, Jornadas de Civil, IST

Rito, A., Cabral, P., & Xavier, L. A (2009). *Nova Ponte sobre o rio Catumbela*, Armando Rito Engenharia SA 1–10.